Journal of the Korean Ceramic Society
Vol. 54, No. 6, pp. 484~491, 2017.

https://doi.org/10.4191/kcers.2017.54.6.08

Evaluations of $Sb_{20}Se_{80-x}Ge_x$ (x = 10, 15, 20, and 25) Glass Stability from Thermal, Structural and Optical Properties for IR Lens Application

Gun-Hong Jung*, Heon Kong*, Jong-Bin Yeo, and Hyun-Yong Lee***,†**

**Department of Advanced Chemicals and Engineering, Chonnam National University, Gwangju 61186, Korea*
***The Research Institute for Catalysis, Chonnam National University, Gwangju 61186, Korea*
****School of Chemical Engineering, Chonnam National University, Gwangju 61186, Korea*

(Received June 30, 2017; Revised September 24, 2017; Accepted October 22, 2017)

ABSTRACT

Chalcogenide glasses have been investigated in their thermodynamic, structural, and optical properties for application in various opto-electronic devices. In this study, the $Sb_{20}Se_{80-x}Ge_x$ with x = 10, 15, 20, and 25 were selected to investigate the glass stability according to germanium ratios. The thermal, structural, and optical properties of these glasses were measured by differential scanning calorimetry (DSC), X-ray diffraction (XRD), and UV-Vis-IR Spectrophotometry, respectively. The DSC results revealed that $Ge_{20}Sb_{20}Se_{60}$ composition showing the best glass stability theoretically results due to a lower glass transition activation energy of 230 kJ/mol and higher crystallization activation energy of 260 kJ/mol. The structural and optical analyses of annealed thin films were carried out. The XRD analysis reveals obvious results associated with glass stabilities. The values of slope *U*, derived from optical analysis, offered information on the atomic and electronic configuration in Urbach tails, associated with the glass stability.

Key words : Glass, Thermal properties, Chalcogenide, Glass stability, Urbach tails

1. Introduction

Chalcogenide glasses are interesting inorganic materials owing to their superior optical transmittance and nonlinear refractive index in the infrared region. They can be used in IR optical devices such as IR lenses, fiber optics, and IR detectors owing to the optical properties.[1-4] They have low cost, balanced optical and mechanical properties, and ease of molding process owing to their glass transition properties.[5-7] To optimize the chalcogenide glass molding process and the reliability about amorphous to crystalline phase transition system, the glass stability in chalcogenide glasses is required owing to the stable amorphous state at the process temperature.

In infrared optics applications, Ge-Sb-Se system chalcogenides are used due to their suitable IR region transmittance, glass stability, mechanical properties, and chemical properties.[8-12] In the Ge-Sb-Se system, we focused that the addition of germanium (Ge) is contributed to glass stabilities due to the resistance to strong tendency for crystallization according to the Sb-Se bonds, which are one of the core parts about glass properties.[11] Therefore, the investigation of glass stability in the wide range of Ge rate is important to optimize the chalcogenide composition for amorphous IR optic applications.

In this study, we investigated the composition for the best glass stability in $Sb_{20}Se_{80-x}Ge_x$ chalcogenide systems by using the thermal, structural, and optical properties. The thermal properties of $Sb_{20}Se_{80-x}Ge_x$ (x = 10, 15, 20, and 25) were investigated by differential scanning calorimetry (DSC, Mattler Toledo DSC823e) analysis under non-isothermal conditions. DSC results were applied by theoretical models (Augis-Bennett, and Kissinger models) to calculate the phase transition activation energy for glass stability. The amorphous to crystalline structural properties and optical properties were studied in X-ray diffractometry (XRD, X'pert PRO Multi Propose X-ray diffractometer) and UV-Vis-NIR Spectrophotometry, respectively.

2. Experimental Procedure

$Sb_{20}Se_{80-x}Ge_x$ chalcogenide bulk glasses, where x = 10, 15, 20 and 25, were fabricated by the well-known melt-quenching method. High purity (99.999%) constituent elements of Ge, Sb, and Se were weighted according to proper atomic weight and then put into a cleaned quartz ampoule. The quartz ampoule for the melt-quenching technique was made of SiO_2 and cleaned successively using nitric acid, sulfuric acid, and iso-propyl alcohol. The element-inserted quartz tubes were vacuum-sealed under 10^{-4} Torr by oxygen welding to prevent oxidation. The sealed ampoules were heated in a tube furnace at 498, 698, 963, and 1233 K for 2 h in consideration of the melting points and the boiling points of each element. Subsequently they were placed at 1273 K for 16 h because of the uniformity of composition. During the melting process, the quartz ampoules were stirred con-

†Corresponding author : Hyun-Yong Lee
E-mail : hyleee@chonnam.ac.kr
Tel : +82-62-530-0803 Fax : +82-62-530-1909

stantly to homogenize the constituents. The samples were quenched in cold water to get a glassy state.

Thin films were deposited by thermal evaporation from the open boat at a deposition rate of ~ 3 Å/s onto chemically cleaned p-type Si (100) and quartz substrates under a vacuum of 3×10^{-5} Torr, and the thickness ratio was measured using a quartz crystal sensor. The film thickness was fixed at ~ 200 nm. The deposited thin films were isothermally annealed at temperatures from 450 K to 630 K with 30 K intervals. The annealing process was performed under a flow of 200 sccm N_2 gas for 30 min at a heating rate of 5 K/min to prevent the oxidation of the thin films.

The thermal properties of bulk samples were studied using the DSC method. The DSC curves were taken under non-isothermal conditions at different heating rates (5, 10, 15, and 20 K/min) on accurately weighted samples sealed in aluminum pans. Each scan was recorded from room temperature to 823 K. The calorimeter was calibrated using the well-known melting temperatures and melting enthalpies of zinc, indium, and gallium (20 mg), crimped into aluminum pans and scanned. To identify the amorphous-to-crystalline phase transition of the annealed $Sb_{20}Se_{80-x}Ge_x$ films, the annealed films were recorded by using XRD with Cu Kα radiation (λ = 1.542 Å).

The optical properties were measured using a UV-VIS-NIR spectrophotometer in the wavelength range ~ 300-1,100 nm. The optical transmittance of the amorphous and crystalline-annealed $Sb_{20}Se_{80-x}Ge_x$ thin films was recorded at room temperature. The absorption coefficient (α) for calculating optical bandgap was measured using the beer-lambert relation as $\alpha = -(1/d)\ln(T)$, where d is the film thickness and T is transmittance of the film.

3. Results and Discussion

Figure 1 shows the DSC curves of $Sb_{20}Se_{80-x}Ge_x$ glasses (x = 10, 15, 20 and 25) at a heating rate of 5 K/min and Fig. 2 is the DSC curves corresponding to heating rate dependences of $Sb_{20}Se_{70}Ge_{10}$ chalcogenide glass. The DSC curves indicate a single glass transition endothermic slope and one or more crystallization exothermic peaks. The single endothermic glass transition confirmed the homogeneity. Fig. 1 shows that the glass transition temperature increased with increasing Ge ratio. The crystallization temperatures increased until the Ge ratio was 20%, and then the value according to 25% of Ge ratio decreased.

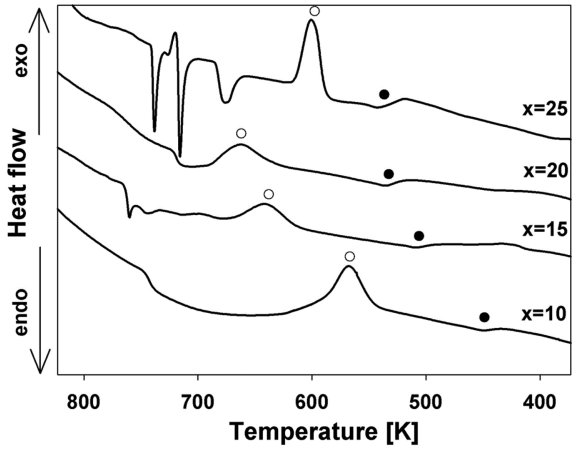

Fig. 1. DSC graphs of the $Sb_{20}Se_{80-x}Ge_x$ (x = 10, 15, 20, and 25) glasses under non-isothermal condition at 5 K/min heating rate. Points of Glass transition (●) and crystallization peak (○) are revealed well in the DSC graph.

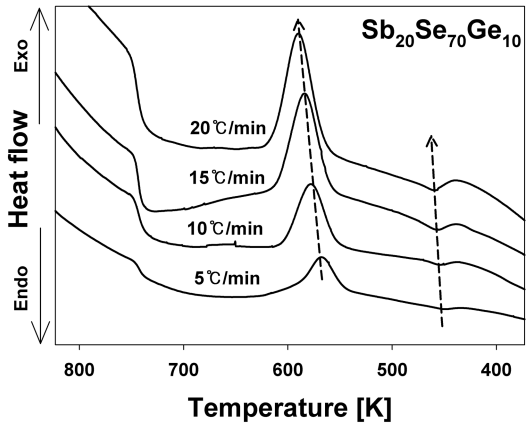

Fig. 2. DSC graphs of the $Sb_{20}Se_{70}Ge_{10}$ chalcogenide glasses at different heating rates of 5, 10, 15, and 20 K/min. The glass transition and crystallization temperatures gradually increased as increasing the heating rates, indicated by dash-line arrows.

The DSC graph parameters of the glass transition temperature (T_g), glass transition endothermic peak temperature (T_{gp}), onset crystallization temperature (T_c), peak crystallization temperature (T_p), and the temperature interval between peak crystallization and glass transition ($T_p - T_g$) are listed in Table 1.

As shown in the Fig. 2 and Table 1, the temperatures T_g and T_c increased gradually as the heating rate (β) increased. This phenomenon according to the T_g is explained using the empirical equation shown in Eq. (1), suggested by Lassocka *et al.*[13]

$$T_g = A + B \ln \beta \quad (1)$$

Where A consists of T_g at a heating rate of 1 K/min, and B is the cooling rate which is taken by the system to reduce the glass transition temperature when the heating rate decreased from 10 K/min to 1 K/min. The plots of T_g versus $\ln \beta$ exhibited a linear relationship, as shown in Fig. 3. The values of A and B are listed in Table 2.

What is the glass transition is one of the issues in the non-crystalline solids. Some authors have given the glass transition as the glass-to-amorphous transition.[14,15] The chalcogenide glass can, therefore, be divide in 'glass' phase and 'amorphous' phase around the point of T_g according to the non-crystal solids. The glass transition region consists of various metastable states separated by energy barriers. The atoms restricted in the metastable states tend to attain

Table 1. The Transition Temperatures According to $Sb_{20}Se_{80-x}Ge_x$ Glasses at the Different Heating Rates

Sample Ge at%	Heating rate [K/min]	T_g [K]	T_{gp} [K]	T_p [K]	T_p–T_g [K]
X = 10	5	435.5	445.5	567.7	131.8
	10	440.8	448.8	578.2	137.8
	15	443.25	453.2	584.3	141.0
	20	444.6	454.6	591.6	147.0
X =15	5	502.8	505.5	640.5	134.9
	10	503.4	509.6	542.5	142.8
	15	503.7	511.2	551.2	147.9
	20	506.0	515.3	559.9	152.6
X = 20	5	527.6	531.2	661.2	133.6
	10	530.4	536.3	672.5	142.1
	15	532.9	542.0	677.2	144.2
	20	533.5	544.3	679.6	146.1
X = 25	5	531.5	536.5	599.2	67.7
	10	535.7	542.3	605.6	69.9
	15	537.2	545.2	607.3	70.1
	20	539.7	548.3	610.0	70.3

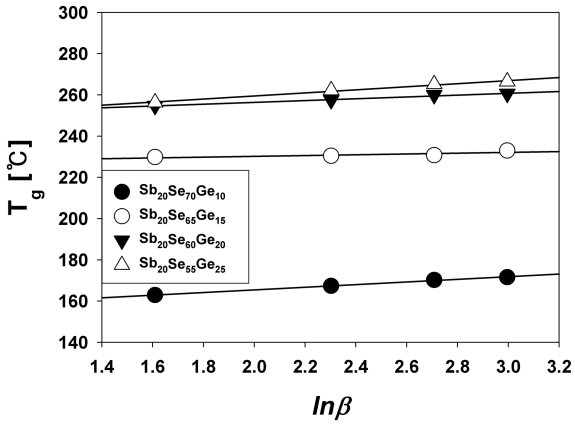

Fig. 3. Glass transition temperature T_g relationship according to the heating rate, lnβ. These linear relationships mean an empirical Lassocka equation.

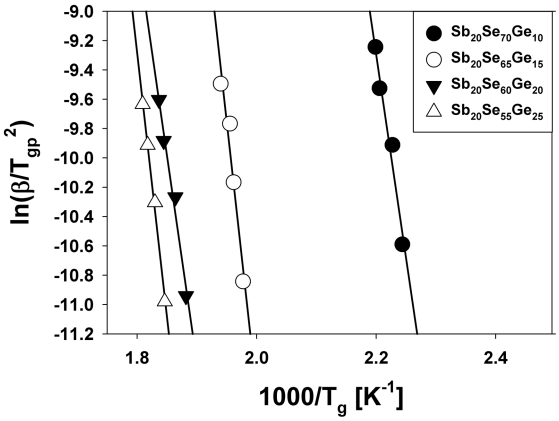

Fig. 4. Plots of $\ln[\beta/T_{gp}^2]$ versus $1000/T_{gp}$.

more stable states than others by overcoming this energy barrier.[16] This energy barrier is known as the activation energy of the glass transition. The lower activation energy of glass transition has a higher probability to jump to the metastable state by the lower energy, which is the most stable state.[17]

The activation energy of glass transition has been evaluated using the Kissinger equation, which is used for the crystallization region. It has also been frequently used for the evaluation of the activation energy of the glass transition.[18,19]

Table 2. The Values of A and B Related to the Lossocka Equation About Different Compositions of Glasses

Sample Ge at%	A [K]	B [min]
X = 10	425.79	6.396
X = 15	499.52	1.932
X = 20	520.65	4.435
X = 25	527.70	7.478

The Kissinger equation optimized for the glass transition is shown by Eq. (2).

$$\ln[\beta/T_{gp}^2] = -E_g/RT_{gp} + const \quad (2)$$

where T_{gp} is the endothermic peak temperature of the glass transition region and R is the universal gas constant. The plots of $\ln[\beta/T_{gp}^2]$ versus $1000/T_{gp}$ are shown in Fig. 4. The activation energy of glass transition (E_g) has been determined from the slope of the plot. The values of E_g according to the various compositions of glasses are listed in Table 3.

The kinetics of the crystallization process under non-isothermal condition has been analyzed in terms of composition dependence of T_c, T_p, and an activation energy of crystallization (E_c). This activation energy considered as the energy according to amorphous to crystalline transformation is the whole process activation energies of the nucleation and the crystal growth.[7] The values of E_c has been evaluated by two different methods under non-isothermal conditions.

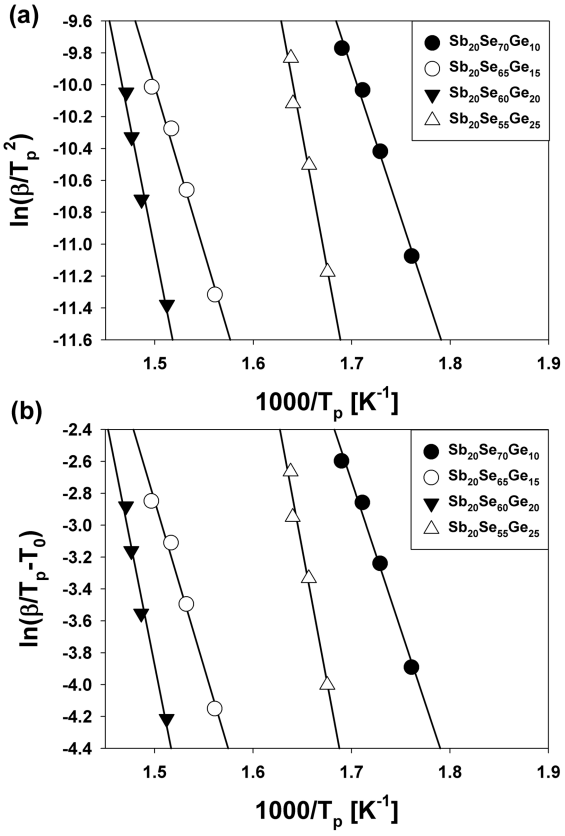

Fig. 5. Plots of (a) ln $[\beta/T_p^2]$ versus $1000/T_p$ corresponding to the Kissinger model and (b) ln $[\beta/(T_p-T_0)]$ versus $1000/T_p$ about the Augis-Bennett model.

First method is the Kissinger equation.[20,21] The values of E_c can be obtained from the dependence of T_p on different heating rates, using Eq. (3) of the Kissinger model. The plots of $\ln[\beta/T_p^2]$ versus $1000/T_p$ are shown in Fig. 5(a) for different glass compositions. The values of E_c can be calculated from the slope of the plots (straight lines)

$$\ln[\beta/T_p^2] = -\Delta E_c/RT_p + \ln[RK_0/\Delta E] \quad (3)$$

The Augis-Benett model was used as another approach with an approximation method to calculate the value of E_c, and the formula of Augis-Benett model is given as Eq. (4).[20,22-24]

$$\ln[\beta/T_p - T_0] = -\Delta E_c/RT_p + \ln K_0 \quad (4)$$

Figure 5(b) shows the plots of $\ln[\beta/(T_p-T_0)]$ versus $1000/T_p$. The slope of straight line gives the E_c. This method has the advantages that the y-intercept of the plot gives the value of the frequency factor (K_0) of the Arrhenius equation.[20,24] The values of E_c and K_0 obtained by two method are listed in Table 3.

As shown in Table 3, the tendencies of the E_g values are divided in two categories: ~ 230 kJ/mol at x = 10 and x = 20 compositions and ~ 300 kJ/mol according to x = 15 and x = 25. The E_g is involved in the molecular motions rearrangements of atoms. It is suggested that a minimum value of E_g has the higher probability to jump to the metastable state of lower configuration energy.[25] In the suggestion, the higher glass forming stability depends on the lower value of E_g. As a result, the compositions of x = 10 and x = 20 have good glass forming ability compared to the composition of x = 15 and x = 25.

The values of E_c are also listed in Table 3. It is well known that the T_c and E_c are important parameters for the characteristics of the thermal stability of amorphous state, and they are considered to be related to the glass forming ability. It is clear from Table 3 that the E_c value increases with increasing Ge content. Especially the value of E_c is rising up from 172 kJ /mol to 260 kJ/mol as the changes of the composition from x = 15 to x = 20. The higher value of E_c has the advantage of anti-crystallization in the range of crystallization-danger intervals, which is an area between T_g and T_c. Once the temperature increase over the T_g, the nucleation occurs in a random fashion at various sites in the samples. After the nuclei grow up to the extent of critical size, the crystal growth is beginning.[26] The higher value of E_c can kinetically impedes the process of nucleation and crystal growth at the crystallization-danger intervals. At the same times, the rate of crystallization is faster, because of decreased temperature range according to the nucleation and growth steps.[22,25] Hence, it is obvious that the chalcogenide glasses with to x = 20 have excellent glass stability in the range between T_g and T_c compared to the x = 15.

Figure 6 shows the XRD patterns of the 30 min-annealed $Sb_{20}Se_{80-x}Ge_x$ chalcogenide thin films. The patterns are arranged by the annealing temperatures. Figs. 6(a) to (d) are corresponding to the compositions of $Sb_{20}Se_{80-x}Ge_x$ chalcogenide thin films from x = 10 to x = 25, respectively. As shown in Fig. 6, crystalline phase peaks appeared at the specific annealing temperatures, and the peaks are formed

Table 3. The Values of Glass Transition, Crystallization Energy, and Frequency Factor using Various Theoretical Models

Sample Ge at%	Glass transition activation energy [kJ/mol]	Crystallization activation energy [kJ/mol]		Frequency factor
	Kissinger	Kissinger	Augis-Bennett	K_0
X = 10	230.80	155.89	154.56	3.48×10^{12}
X = 15	305.70	172.43	172.59	1.95×10^{12}
X = 20	235.04	259.39	259.81	4.73×10^{18}
X = 25	282.84	384.27	383.52	4.71×10^{31}

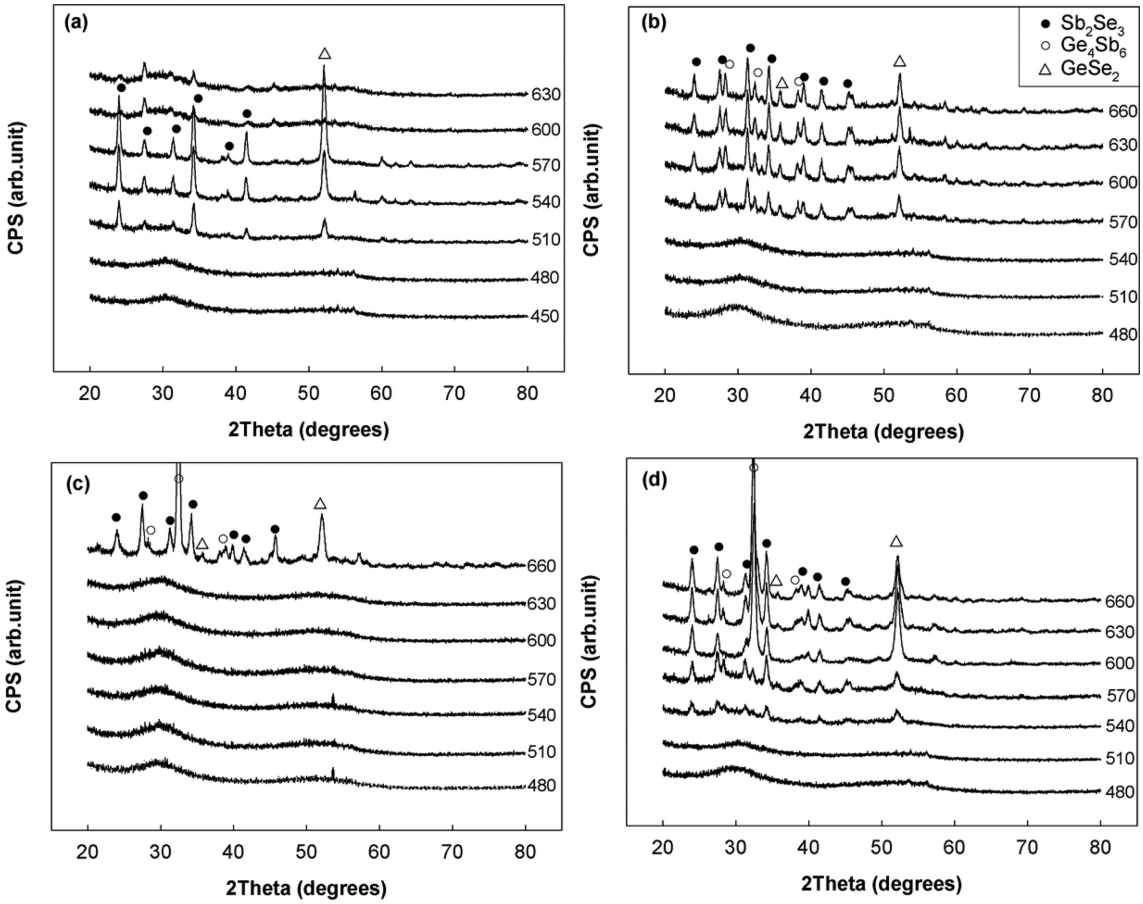

Fig. 6. XRD graphs according to $Sb_{20}Se_{80-x}Ge_x$ thin films. Figs. 6(a) to (d) correspond to compositions from x = 10 to x = 25, respectively, at different annealing temperatures from 480 K to 660 K excepting $Sb_{20}Se_{70}Ge_{10}$. According to $Sb_{20}Se_{70}Ge_{10}$ thin films, the surface of the thin films started to melt and destroyed from 600 K. For the reason, the annealing temperatures are lower than the others.

with increasing temperature. The crystalline phases consist of Sb_2Se_3, $GeSe_2$, and Ge_4Sb_6.[27,28] Fig. 6(a) onlyshows the Sb_2Se_3 and $GeSe_2$ crystalline phase peaks because of the relatively lower Ge contents. In the Ge-Sb-Se chalcogenide system, it is suggested that the elements of the system prefer heteropolar bonds compared to homopolar bond. Furthermore, the heteropolar bonds are preferred to Sb_2Se_3, $GeSe_2$, and Ge_4Sb_6, in order. Therefore, with increasing Ge contents, the crystalline peaks according to $GeSe_2$ and Ge_4Sb_6 appear and increase in intensity. Comparing the composition of $Sb_{20}Se_{65}Ge_{15}$ with $Sb_{20}Se_{60}Ge_{20}$, the crystallization temperatures according to the compositions do not have much difference in the DSC result as shown in Fig. 1 and Table 3. However, as shown in Figs. 6(b) and (c), the temperatures of crystallization have the obvious temperature gap. This phenomenon considers that the composition of $Sb_{20}Se_{65}Ge_{15}$ glasses has lower glass forming ability and glass stability than the composition of $Sb_{20}Se_{60}Ge_{20}$ glasses, suggested by the result of thermal analysis.

Amorphous chalcogenides with a strong electron-lattice interaction obey the absorption properties expressed as $ahv = B(hv - E_{op})^n$ for the extended energy region ($hv > E_{op}$) and lies in the range ~ 10^3 $cm^{-1/2}$ $eV^{-1/2}$.[29-32] B and E_{op} mean the slope of extended region and optical bandgap, respectively. Moreover, the U represents the slope of the Urbach tail region ($hv < E_{op}$).[33] The exponent n is an appropriate and selected index, depending on the nature of electronic transition and can be assumed to have a value of either 1/2 or 2 for the direct and indirect transition, respectively.[34] Many studies have shown $n = 2$ acceptable for amorphous chalcogenides, including GeSe, GeSbTe and GeSbSe.[27,35-37]

Therefore, E_{op} is obtained from the intercept on the energy axis of the plot $(ahv)^{1/2}$ versus hv as shown in Fig. 7. Figs. 7 (a), (b), (c), and (d) correspond to the composition of the $Sb_{20}Se_{70}Ge_{10}$, $Sb_{20}Se_{65}Ge_{15}$, $Sb_{20}Se_{60}Ge_{20}$ and $Sb_{20}Se_{55}Ge_{25}$, respectively. The quantities of E_{op}, $B^{1/2}$ and U for the amorphous and crystalline-onset $Sb_{20}Se_{80-x}Ge_x$ were determined from Fig. 7 and are summarized in Table 4. The annealing temperatures according to crystalline-onset were applied from the XRD data.

As shown in Fig. 7 and Table 4, The E_{op} quantities of $Sb_{20}Se_{80-x}Ge_x$ (x = 10, 15, 20, and 25) amorphous films were ~ 1.62, 1.77, 1.55, and 1.39 eV, respectively. The $Sb_{20}Se_{65}Ge_{15}$ composition exhibits the largest value of E_{op}, suggesting

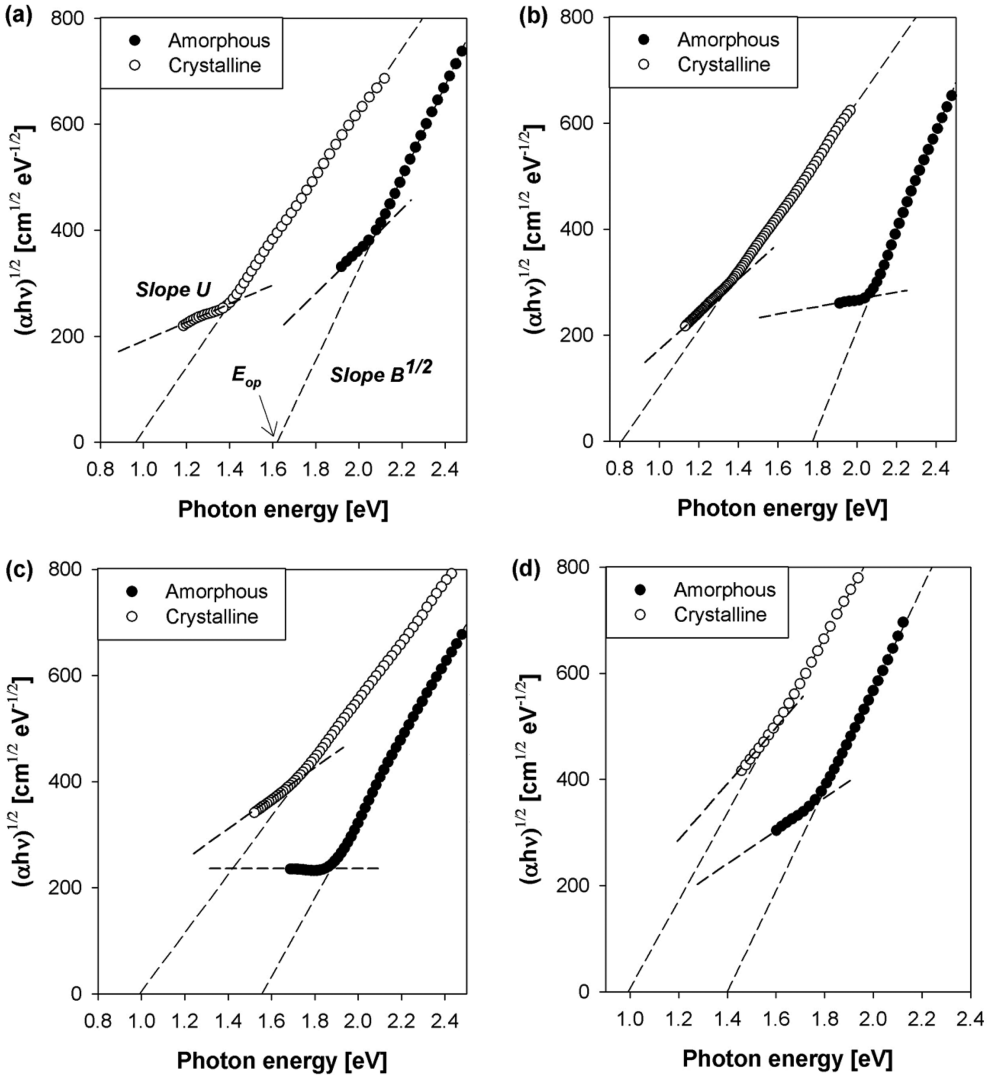

Fig. 7. plot $(ahv)^{1/2}$ versus hv. (a), (b), (c) and (d) are corresponding to the composition of the $Sb_{20}Se_{70}Ge_{10}$, $Sb_{20}Se_{65}Ge_{15}$, $Sb_{20}Se_{60}Ge_{20}$ and $Sb_{20}Se_{55}Ge_{25}$, respectively. The quantities of $B^{1/2}$ and U according to the amorphous and crystalline-onset $Sb_{20}Se_{80-x}Ge_x$ were determined by slope of the graph

that the $Sb_{20}Se_{65}Ge_{15}$ approaches the stoichiometric compositions in the $Sb_{20}Se_{80-x}Ge_x$ systems.[38] In the stoichiometric composition, the heteropolar bands are larger than the homopolar bands, leading the average bond energy to the maximum state.[27] After crystallization, the whole values of E_{op} decrease rapidly in the range ~ 0.8 - 1 eV. Two slopes $B^{1/2}$ and U offer information on the atomic and electronic configuration in the extended and Urbach region, respectively. A slope reduction has been reported because of increasing of randomness in the atomic configuration.[39] The values of U are listed in Table 4 and shown in Fig. 7. The lower value of U in the amorphous state means the superior heat confinement due to the large band-tail state.[32] It may be regarded as the glass stability. The higher heat confinement means the acceptance of higher temperature, maintaining the glassy state. The $Sb_{20}Se_{65}Ge_{15}$ and $Sb_{20}Se_{60}Ge_{20}$ have sufficiently lower U values of 68 and 8 $cm^{-1/2}$ $eV^{-1/2}$, respectively, compared to the others with ~ 300 $cm^{-1/2}$ $eV^{-1/2}$. At the same times, they have a higher crystallization temperature than the others as shown by the result of thermal analysis. $Sb_{20}Se_{60}Ge_{20}$ composition has the lowest U of 8 $cm^{-1/2}$ $eV^{-1/2}$ as compared to $Sb_{20}Se_{65}Ge_{15}$. Hence, it is possible to accept more heat energy then the other compositions.

Table 4. Optical Parameters, E_{op}, $B^{1/2}$, and U for Amorphous and Crystalline $Sb_{20}Se_{80-x}Ge_x$ Thin Films

Sample Ge at%	phase	E_{op} [eV]	$B^{1/2}$ [$cm^{-1/2}eV^{-1/2}$]	U [$cm^{-1/2}eV^{1/2}$]
X = 10	Amorphous	1.62	861	387
	Crystalline	0.96	600	168
X = 15	Amorphous	1.77	927	68
	Crystalline	0.82	536	364
X = 20	Amorphous	1.55	740	8
	Crystalline	0.99	549	326
X = 25	Amorphous	1.39	953	377
	Crystalline	0.99	825	592

Therefore, $Sb_{20}Se_{60}Ge_{20}$ composition has the best glass stability.

4. Conclusions

The glass stability of $Sb_{20}Se_{80-x}Ge_x$ (x = 5, 10, 15, and 20) was investigated by thermal, structural, and optical analyses. The DSC curves of $Sb_{20}Se_{60}Ge_{20}$ showed the highest crystallization temperature. The kinetics according to the glass transition and crystallization was investigated by the Kissinger and Augis-bennett models. These models exhibited $Sb_{20}Se_{60}Ge_{20}$ composition with good glass forming ability and excellent glass stability at once. The XRD results revealed that $Sb_{20}Se_{60}Ge_{20}$ glass had the best glass stability by the results of the crystalline-revealed temperature of the annealed thin films. Through the optical analysis, the quantities of *U* were related to the glass stability, and the results agreed well with the DSC and XRD results.

Acknowledgments

This research was supported by the Basic Science Research Program through the National Research Foundation of Korea (NRF) funded by the Ministry of Science and ICT (No. NRF-2016R1A2B4014848).

REFERENCES

1. X. Gai, T. Han, A. Prasad, S. Madden, D. Choi, R. P. Wang, D. Bulla, and B. Luther-Davies, "Progress in Optical Waveguides Fabricated from Chalcogenide Glasses," *Opt. Express,* **18** [25] 26635-46 (2010).
2. B. Luo, Y. Wang, Y. Sun, S. Dai, P. Yang, P. Zhang, X. Wang, F. Chen, and R. Wang, "Fabrication and Characterization of Bare Ge-Sb-Se Chalcogenide Glass Fiber Taper," *Infrared Phys. Technol.*, **80** 105-11 (2017).
3. G. G. Devyatykh and E. M. Dianov, "Research In KRS-5 And Chalcogenide Glass Fibers," *SPIE PROC.*, **484** 105 (1984).
4. K. J. Ma, H. H. Chien, S. W. Huang, W. Y. Fu, and C. L. Chao, "Contactless Molding of Arrayed Chalcogenide Glass Lenses," *J. Non-Cryst. Solids,* **357** 2484-88 (2011).
5. D. H. Cha, J. H. Kim, and H. J. Kim, "Molding and Evaluation of Ultra-Precision Chalcogenide-Glass Lens for Thermal Imaging Camera Using Thermal Deformation Compensation (*in Korean*)", *J. KIEEME*, **27** [2] 91-6 (2014).
6. D. S. Bae, J. B. Yeo, and H. Y. Lee, "A Study on a Production and Processing Technique for a GeSbSe Aspheric Lens with a Mid-infrared Wavelength Band," *J. Korean Phys. Soc.*, **62** [11] 1610-15 (2013).
7. A. K. Singh, "Crystallization Kinetics of Chalcogenide Glasses," pp. 29-64 in Crystallization - Science and Technology, Ed. by B. Andreeta, InTech, 2012.
8. M. Saxena, "A Crystallization Study of Amorphous $Te_x(Bi_2Se_3)_{1-x}$ Alloys with Variation of the Se Content," *J. Phys. D: Appl. Phys.*, **38** [3] 460-63 (2005).
9. P. Sharma, I. Sharma, and S. C. Katyal, "Physical and Optical Properties of Binary Amorphous Selenium-Antimony Thin Films," *J. Appl. Phys.*, **105** [5] 053509 (2009).
10. D. Tonchev and S. O. Kasap, "Thermal Properties of Sb_xSe_{100-x} Glasses Studied by Modulated Temperature Differential Scanning Calorimetry," *J. Non-Cryst. Solids*, **248** [1] 28-36 (1999).
11. S. Sharda, N. Sharma, P. Sharma, and V. Sharma, "Band Gap and Dispersive Behavior of Ge Alloyed a-SbSe Thin Films Using Single Transmission Spectrum," *Mater. Chem. Phys.*, **134** 158-62 (2012).
12. W. H. Wei, R. P. Wang, X. Shen, L. Fang, and L. D. Barry, "Correlation between Structural and Physical Properties in Ge-Sb-Se Glasses," *J. Phys. Chem. C*, **117** [32] 16571-76 (2013).
13. M. Lasocka, "The Effect of Scanning Rate on Glass Transition Temperature of Splat-Cooled $Te_{85}Ge_{15}$," *Mater. Sci. Eng.*, **23** [2-3] 173-76 (1976).
14. A. H. Moharram, A. A. Abu- Sehly, M. A. El-Oyoun, and A. S. Slotan, "Pre-Crystallization and Crystallization Kinetics of Some Se-Te-Sb Glasses," *Phys. B,* **324** [1-4] 344-51 (2002).
15. N. Mehta and A. Kumar, "Critical Analysis of Endo-Thermal Effect in the Glass Transition Process in Chalcogenide Glasses," *J. Non-Cryst. Solids,* **358** [20] 2783-87 (2012).
16. A. Kaswan, V. Kumari, D. Patidar, N. S. Saxena, and K. Sharma, "Kinetics of Phase Transformations and Thermal Stability of $Ge_xSe_{70}Sb_{30-x}$ (x = 5, 10, 15, 20) Chalcogenide Glasses," *New J. Glass Ceram.*, **2013** [3] 99-103 (2013).
17. M. M. A. Imran, D. Bhandari, and N. S. Saxena, "Enthalpy Recovery during Structural Relaxation of $Se_{96}In_4$ Chalcogenide Glass," *Phys. B*, **293** [3-4] 394-401 (2001).
18. H. E. Kissinger, "Variation of Peak Temperature with Heating Rate in Differential Thermal Analysis," *J. Res. Natl. Bur. Stand.*, **57** [4] 217-21 (1956).
19. H. S. Chen, "A Method for Evaluating Viscosities of Metallic Glasses from the Rate of Thermal Transformations," *J. Non-Cryst. Solids*, **27** [2] 257-63 (1978).
20. J. A. Augis, J. E. Bennett, "Calculation of the Avrami Parameters for Heterogeneous Solid State Reactions Using a Modification of the Kissinger Method," *J. Therm. Anal.*, **13** [2] 283-92 (1978).
21. H. E. Kissinger, "Reaction Kinetics in Differential Thermal Analysis," *J. Anal. Chem.*, **29** [11] 1702-6 (1957).
22. M. Avrami, "Kinetics of Phase Change. I. General Theory," *J. Chem. Phys.*, **7** [12] 1103-12 (1939).
23. M. Avrami, "Kinetics of Phase Change. II. Transformation-Time Relations for Random Distribution of Nuclei," *J. Chem. Phys.*, **8** [2] 212 (1940).
24. M. Muiva, T. Stephan, and M. Julius, "Crystallisation Kinetics, Glass Forming Ability and Thermal Stability in Glassy $Se_{100-x}In_x$ Chalcogenide Alloys," *J. Non-Cryst. Solids*, **357** [22-23] 3726-33 (2011).
25. A. A. Al-Ghamdi, M. A. Alvi, and S. A. Khan, "Non-Isothermal Crystallization Kinetics Study on $Ga_{15}Se_{85-x}Ag_x$ Chalcogenide Glasses by Using Differential Scanning Calorimeter," *J. Alloys Compd.*, **509** [5] 2087-93 (2011).
26. N. Mehta, R. S. Tiwari, and A. Kumar, "Glass Forming Ability and Thermal Stability of Some Se-Sb Glassy

Alloys," *Mater. Res. Bull.*, **41** [9] 1664-72 (2006)
27. A. A. Abu-Sehly and A. S. Soltan, "Optical Properties and Structure of $Ge_{20}Sb_xSe_{80-x}$ Films," *Appl. Surf. Sci.*, **199** [1-4] 147-59 (2002).
28. M. A. Abedl-Rahim, A. H. Moharram, M. Dongol, and M. M. Hafiz, "Experimental Studies of the Ge-Sb-Se System," *J. Phys. Chem. Solids*, **51** [4] 355-59 (1990).
29. H. Y. Lee, S. H. Park, J. Y. Chun, and H. B. Chung, "Photoinduced Transformations in Amorphous $Se_{75}Ge_{25}$ Thin Film by XeCl Excimer-Laser Exposure," *J. Appl. Phys.*, **83** [10] 5381 (1998).
30. K. Tanaka, "Reversible Photostructural Change: Mechanisms, Properties and Applications," *J. Non-Cryst. Solids*, **35-36** 1023-34 (1980).
31. N. F. Mott and E. A. Davis, Electron Process in Non-Crystalline Materials; pp. 199-319, 2nd ed., Oxford University Press, New York, 1979.
32. H. Y. Lee and H. B. Chung, "Low-Energy Focused-Ion-Beam Exposure Characteristics of an Amorphous $Se_{75}Ge_{25}$ Resist," *J. Vac. Sci. Technol. B*, **15** [4] 818 (1997).
33. F. Urbach, "The Long-Wavelength Edge of Photographic Sensitivity and of the Electronic Absorption of Solids," *Phys. Rev.*, **92** 1324 (1953).
34. B. Gürbulak, S. Duman, and A. Ates, "The Urbach Tails and Optical Absorption in Layered Semiconductor $TiGaSe_2$ and $TiGaSe_2$ Single Crystal," *Czech. J. Phys.*, **55** [1] 93-103 (2005).
35. B. S. Lee, J. R. Abelson, S. G. Bishop, D. H. Kang, B. K. Cheong, and K. B. Kim, "Investigation of the Optical and Electronic Properties of $Ge_2Sb_2Te_5$ Phase Change Material in its Amorphous, Cubic, and Hexagonal Phases," *J. Appl. Phys.*, **97** 093509 (2005).
36. H. Y. Lee, J. W. Kim, and H. B. Chung, "Evaluation for the Photo-Induced Changes of Photoluminescence and Optical Energy Gap in Amorphous $Se_{100-x}Ge_x$ (x = 5, 25, and 33) Thin Films," *J. Non-Cryst. Solids*, **315** [3] 288-96 (2003).
37. K. H. Song, S. W. Kim, J. H. Seo, and H. Y. Lee, "Influence of the Additive Ag for Crystallization of Amorphous Ge-Sb-Te Thin Films," *Thin Solid Films*, **517** [4] 3958-62 (2009).
38. W. H. Wei, R. P. Wang, X. Shen, L. Fang, and B. Luther-Davies, "Correlation between Structural and Physical Properties in Ge-Sb-Se Glasses," *J. Phys. Chem. C*, **117** [32] 16571-76 (2013).
39. Y. Utsugi and Y. Mizushima, "Photostructural Change in the Urbach Tail in Chalcogenide Glasses," *J. Appl. Phys.*, **51** 1773 (1980).